Article ID: 1000-324X(2023)04-0452-09 **DOI:** 10.15541/jim20220542

Fabrication and Microstructure of Gd_2O_2S:Tb Scintillation Ceramics from Water-bath Synthesized Nano-powders: Influence of H_2SO_4/Gd_2O_3 Molar Ratio

WU Junlin[1,2], DING Jiyang[1,3], HUANG Xinyou[3], ZHU Danyang[1,2], HUANG Dong[1,3], DAI Zhengfa[1], YANG Wenqin[4,5], JIANG Xingfen[4,5], ZHOU Jianrong[4,5], SUN Zhijia[4,5], LI Jiang[1,2]

(1. Key Laboratory of Transparent Opto-functional Inorganic Materials, Shanghai Institute of Ceramics, Chinese Academy of Sciences, Shanghai 201899, China; 2. Center of Materials Science and Optoelectronics Engineering, University of Chinese Academy of Sciences, Beijing 100049, China; 3. School of Material Science and Engineering, Jiangsu University, Zhenjiang 212013, China; 4. Spallation Neutron Source Science Center, Dongguan 523803, China; 5. State Key Laboratory of Particle Detection and Electronics, Institute of High Energy Physics, Chinese Academy of Sciences, Beijing 100049, China)

Abstract: The Gd_2O_2S:Tb scintillation ceramics is extensively used for neutron radiography and industrial non-destructive testing due to its bright green emission, high intrinsic conversion efficiency and high thermal neutron capture cross-section. However, the existence of Gd_2O_3 secondary phase in Gd_2O_2S ceramics impedes the scintillation property. In this work, The Gd_2O_2S:Tb precursors were synthesized in water-bath with H_2SO_4 and Gd_2O_3 as starting materials. Molar ratio of H_2SO_4 to Gd_2O_3 defined as n was adjusted to synthesize the precursors., which influence on the properties of the precursors and powders was studied. Chemical composition of the precursors changes with the increase of n, from $2Gd_2O_3{\cdot}Gd_2(SO_4)_3{\cdot}xH_2O$ (n<2.00) to $Gd_2O_3{\cdot}2Gd_2(SO_4)_3{\cdot}xH_2O$ (2.25≤n≤2.75), and to $Gd_2(SO_4)_3{\cdot}8H_2O$ (n=3.00). After being calcined and reduced, all the powders form pure Gd_2O_2S phase. Morphology of the Gd_2O_2S:Tb powders is closely related to the phase composition of the precursor. Increasement of the XEL intensity shows two stages with n increase, corresponding to the phase transition of the precursor, respectively. The Gd_2O_2S:Tb scintillation ceramics were therefore fabricated by vacuum pre-sintering and HIP post-treatment. The ceramics were fabricated from the powders prepared with different n, achieving high relative density and XEL intensity, except the ceramics fabricated from the powders prepared with the n=2.00, 2.25, 2.50. The increase of n is beneficial to the removal of the Gd_2O_3 secondary phase from the Gd_2O_2S:Tb ceramics. This work provides a way for eliminating the secondary phase in Gd_2O_2S:Tb scintillation ceramics.

Key words: water-bath method; molar ratio of H_2SO_4 to Gd_2O_3; Gd_2O_2S:Tb nanopowder; scintillation ceramics

Inorganic scintillation materials have been applied in many fields such as X-rays medical imaging, high energy physics and industrial manufacturing[1-5]. Gadolinium oxysulfide (Gd_2O_2S) is an efficient and excellent matrix to produce phosphors and scintillation ceramics for luminescence and scintillation applications[6-7], due to its wide bandgap (4.6–4.8 eV)[8], high density (7.34 g/cm^3)[9], and high chemical stability[10]. However, the Gd_2O_2S single crystal with high optical and scintillation quality, meeting the requirements of practical application, has not been reported. While, the Gd_2O_2S-based phosphors have attracted considerable attention for decades[11-14]. For instance, Terbium doped gadolinium oxysulfide (Gd_2O_2S:Tb) phosphor exhibits intensive green emission and high luminous efficiency[15-16], which makes it widely used for display purposes in TV screens, cathode ray tubes, and X-ray intensifying screens[17-21]. The Gd_2O_2S:Tb, applied for scintillation screens, mainly includes powder and

Received date: 2022-09-16; **Revised date:** 2022-10-13; **Published online:** 2022-12-30
Foundation item: National Natural Science Foundation of China (12175254, U1832119); National Key R&D Program of China (2021YFE0104800); International Partnership Program of Chinese Academy of Sciences (121631KYSB20200039); International Cooperation Project of Shanghai Science and Technology Commission (20520750200); National Centre for Research and Development (WPC2/1/SCAPOL/2021)
Biography: WU Junlin (1998–), male, Master candidate. E-mail: wujunlin20@mails.ucas.ac.cn
吴俊林(1998–), 男, 硕士研究生. E-mail: wujunlin20@mails.ucas.ac.cn
Corresponding author: LI Jiang, professor. E-mail: lijiang@mail.sic.ac.cn
李 江, 研究员. E-mail: lijiang@mail.sic.ac.cn

ceramic scintillators[22-24]. However, for the powder scintillation screen[25], the poor thermal performance and radiation hardness limit its service lifespan. Due to the boundary scattering and the difference of refractive index among bubbles, powder particles and binders, the light output and optical uniformity are reduced. In contrast, ceramic scintillation screens can solve these problems well and effectively improve the light output. However, it is difficult to obtain high transparent ceramics for the birefringence caused by non-cubic structure[26].

Gd_2O_2S belongs to hexagonal system (space group P3-m1 and lattice parameters a=b=0.3851 nm, c= 0.6664 nm)[27]. Each oxygen ion is surrounded by three gadolinium ions, while each sulfur ion is coordinated by six gadolinium ions to form a stable structure[28-29]. However, the binding force of Gd toward S is much lower than that of O according to the hard and soft acid and base (HSAB) theory[30]. As a result, the secondary phase of Gd_2O_3 is easily produced during the preparation of Gd_2O_2S ceramics. So, avoiding the existence of Gd_2O_3 is the main task of the Gd_2O_2S ceramics fabrication. At present, there are mainly two ways to synthesize Gd_2O_2S powders[26]. One is to "supplement" the S element into the structure of Gd_2O_3. The other one is to synthesize the precursors which are calcined to provide $Gd_2O_2SO_4$, and then the $Gd_2O_2SO_4$ is reduced to Gd_2O_2S powders. In general, the sulfur supplementation method involves complicated procedures, high reaction temperatures and environmentally harmful sulfurization reagents such as S, CS_2, H_2S[31-32]. The method produces micron-sized particles of irregular and uncontrolled morphologies[33]. The reduction method usually involves mild reaction conditions, fewer by-products, and can obtain powders with smaller particles[34-35]. The fine precursor powders can react more sufficiently in the reduction process, improving the uniformity of components[36-37]. Meanwhile, the powders are conducive to the uniformity of ceramics sintering, and can reduce the formation of the secondary phase. The water-bath method is one of the reduction methods, which has the advantages of simple process and harmless by-products. Recently our group used the water-bath method to synthesize Gd_2O_2S powders[34,36,38]. The morphology of the powders produced by the reduction method depends largely on the morphology of the precursors. The morphology, composition of the precursors can be affected by many factors, such as bathing temperature and time, volume of solution, solution pH and the molar ratio of H_2SO_4 to Gd_2O_3[39-41]. The secondary phase of Gd_2O_3 in Gd_2O_2S ceramics is caused by the volatilization of sulfur. So, changing n is an effective strategy to make appropriate sulfur supplement in the process of synthesizing precursors. Different n produce precursors with different chemical components, which change the morphology and property of the powders.

In this work, n was adjusted to synthesize the precursors in the water-bath method. Gd_2O_2S:Tb nanopowders were obtained *via* reducing in flowing mixture of argon and hydrogen (H_2-Ar). The chemical composition and phase evolution of the precursors were analyzed in detail. The influence of n on the morphology and X-ray excited luminescence (XEL) spectrum of the Gd_2O_2S:Tb powders were investigated. Gd_2O_2S:Tb scintillation ceramics were fabricated by the two-step sintering method comprised of vacuum pre-sintering and hot isostatic pressing (HIP) post-treatment. The influences of n on the chemical composition, morphology and microstructure of the Gd_2O_2S:Tb ceramics were investigated. The microstructure and chemical homogeneity of the obtained ceramics were analyzed by FESEM and EDS. The luminescence properties of the Gd_2O_2S:Tb ceramics were evaluated as well.

1 Experimental

The starting materials were commercial oxide powders: Gd_2O_3 (99.999%, Zhongkai New Materials Co., Ltd., Jining, China), Tb_4O_7 (99.995%, Zhongkai New Materials Co., Ltd., Jining, China) and concentrated H_2SO_4 (AR, Sinopharm Chemical Reagent Co., Ltd., Shanghai, China). $Tb(NO_3)_3$ solution was prepared by dissolving Tb_4O_7 in hot nitric acid. Gd_2O_3 was mixed with $Tb(NO_3)_3$ together in stoichiometric ratios of $(Gd_{0.995}Tb_{0.005})_2O_2S$. Then dilute H_2SO_4 solutions with different n were added to the suspension at 7 ℃ at a dripping speed of 8 mL/min. n was adjusted to 1.00, 1.25, 1.50, 1.75, 2.00, 2.25, 2.50, 2.75 and 3.00. After the reaction was conducted at 90 ℃ for 2 h in quartz beaker, the precursors were collected *via* centrifugation, and then dried in an oven at 70 ℃ for 48 h. The precursors were calcined in a tube furnace under flowing H_2-Ar. The Gd_2O_2S:0.5%Tb (in atomic) powders were uniaxially pressed into pellets of 18 mm in diameter at 30 MPa and then cold isostatically pressed under 250 MPa. For ceramics fabrication, the green pellets were pre-sintered at 1300 ℃ for 3 h in vacuum and subsequently HIP post-treated at 1450 ℃ for 3 h under 176 MPa in Ar atmosphere. At last, the samples were double-face polished to 1 mm thickness.

Phase identification was identified by the X-ray diffractometry (XRD, D/max2200 PC, Rigaku, Japan) using Cu Kα radiation (λ=0.15406 nm) with a scanning speed of 5 (°)/min in the 2θ range of 10°–80°. The

morphologies of the reduced powders were observed by the field emission scanning electron microscope (FESEM, SU9000, Hitachi, Japan). The microstructures of the Gd_2O_2S:Tb ceramics were observed by a field emission scanning electron microscope (FESEM, SU8220, Hitachi, Japan). The chemical compositions of the ceramics were analyzed by the energy dispersive spectrum (EDS). X-ray excited luminescence (XEL) spectra were recorded by a homemade XEL spectrometer using a F30III-2 X-ray tube performed at 75 kV voltage and 1.5 mA current with a tungsten target and an Ocean Optics QE65000 collector.

2 Results and discussion

Fig. 1 shows the XRD patterns of the precursors after the reaction of H_2SO_4 and Gd_2O_3 with different n in hot water bath at 90 ℃ for 2 h. For the precursors with n<2.00, all the precursors with similar diffraction patterns were obtained, indicating that the amount of sulfuric acid is not enough to make the occurrence of precursor phase transition. And the composition of the precursors can be formulated as $2Gd_2O_3{\cdot}Gd_2(SO_4)_3{\cdot}xH_2O$[42]. However, with the increase of n, some significant changes occurred in the diffraction peaks of the precursors, and the diffraction peaks of $Gd_2(SO_4)_3{\cdot}8H_2O$ appear gradually. As reported in an American patent, the composition of the precursor is $Gd_2O_3{\cdot}2Gd_2(SO_4)_3{\cdot}xH_2O$ with n= 2.00–2.75, but it was not described in detail[43]. For the precursor with n=3.00, all characteristic diffraction peaks of the precursor correspond well to the $Gd_2(SO_4)_3{\cdot}8H_2O$ (PDF#31-0535). The precursor is consistent with the product of the complete reaction of H_2SO_4 and Gd_2O_3 with stoichiometric ratio of 3 ∶ 1. According to the above results, with the increase of sulfuric acid usage, theproportion of SO_4^{2-} in the precursor increases. Considering the easy loss of S element in the preparation of Gd_2O_2S powders, it is beneficial to replenish the sulfur in the powders.

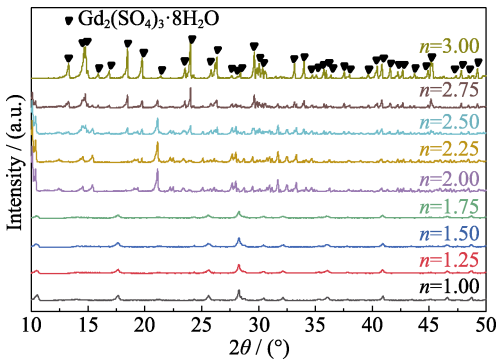

Fig. 1 XRD patterns of the products prepared with different n of H_2SO_4 and Gd_2O_3 in hot water bath at 90 ℃ for 2 h

Then the precursors were calcined in air at 600 ℃ for 3 h, and the phase composition of the calcined products were characterized, as shown in Fig. 2. It can be seen that the diffraction peaks of the products with n<2.00 correspond well to the orthorhombic structured $Gd_2O_2SO_4$ (PDF#29-0613). For the products with n=2.00–2.75, two phases of $Gd_2O_2SO_4$ and $Gd_2(SO_4)_3$ appeared after being calcined in air. And the increase of n leads to an increase in the XRD diffraction intensity of $Gd_2(SO_4)_3$, which is due to the appearance of $Gd_2(SO_4)_3{\cdot}8H_2O$ phase in the precursor. It is noteworthy that the precursor with n=3.00 is completely transformed into pure $Gd_2(SO_4)_3$, because diffraction peaks of the product correspond well to $Gd_2(SO_4)_3$ (PDF#39-0306). The reaction process of the precursors with different n calcined in air can be expressed as:

n<2.00:

$$2Gd_2O_3\cdot Gd_2(SO_4)_3 \rightarrow 3Gd_2O_2SO_4 \quad (1)$$

2.00≤n≤2.5:

$$Gd_2O_3\cdot 2Gd_2(SO_4)_3 \rightarrow \frac{3}{2}Gd_2O_2SO_4 + \frac{3}{2}Gd_2(SO_4)_3 \quad (2)$$

n>2.50:

$$Gd_2(SO_4)_3\cdot 8H_2O \rightarrow Gd_2(SO_4)_3 + 8H_2O \quad (3)$$

Fig. 3 shows the XRD patterns of the Gd_2O_2S:Tb powders with different n. After being calcined at 750 ℃ under hydrogen atmosphere, all diffraction peaks of the powders correspond well to the hexagonal crystal structure of Gd_2O_2S (PDF#26-1422). Although the phase transitions of the precursors calcined in air are different to some extent, the phase compositions of the final powders are almost the same without any secondary phases observed. However, the XRD diffraction intensity of Gd_2O_2S:Tb powders changes with the composition of the precursors, which indicates that the crystallinity of the powders has changed. Theoretically, Gd_2O_2S:Tb powders with n≥2.00 have higher purity compared to others, because of the occurrence of following reactions:

$$Gd_2O_2SO_4 + 4H_2 \rightarrow Gd_2O_2S + 4H_2O \quad (4)$$

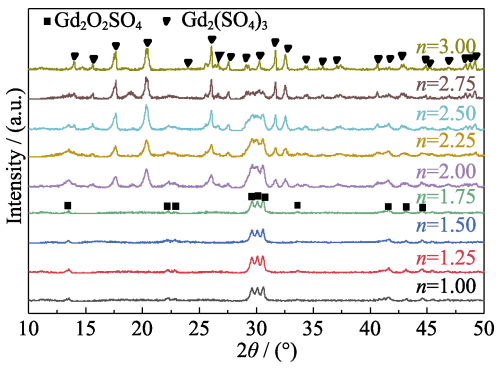

Fig. 2 XRD patterns of the products calcined in air at 600 ℃ for 3 h from the precursors prepared with different n

$$Gd_2(SO_4)_3 + 12H_2 \rightarrow Gd_2O_2S + 10H_2O + 2H_2S \quad (5)$$

H_2S produced during reduction can not only inhibit the volatilization of S element, but also play a role in sulfidation, which is beneficial to the preparation of high purity Gd_2O_2S powder.

Fig. 4 shows the FESEM micrographs of Gd_2O_2S:Tb powders with different n. It can be seen that all Gd_2O_2S:Tb powders present layered or block structure with severe agglomeration. The fact that the reduced Gd_2O_2S:Tb powder retains the overall morphology of thecomposition, presenting overlapping and interlaced layered structures. With the component transformation of the precursor (*i.e.* the increase of SO_4^{2-} content in the precursor components), Gd_2O_2S:Tb powders gradually

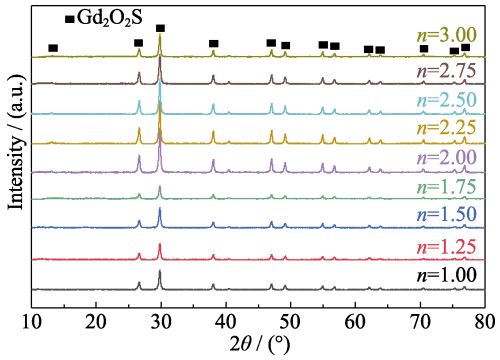

Fig. 3　XRD patterns of the products calcined in air and reduced in H_2 at 750 ℃ for 2 h from the precursors prepared with different n

precursor has been confirmed by our previous work. And it can be found from Fig. 1 and Fig. 4 that the morphology of the Gd_2O_2S:Tb powder is closely related to the phase composition of the precursor. Namely, the composition of the precursor determines the morphology of the reduced powder. For example, all Gd_2O_2S:Tb powders with n<2.00 have the same chemical
show a superposed block structure, which is attributed to the bonding action of the SO_4^{2-} groups.

The XEL spectra of Gd_2O_2S:Tb powders with different n were measured and compared with the commercial micron Gd_2O_2S:Tb powders, as shown in Fig. 5. In Fig. 5(a), the characteristic emission peaks of Tb^{3+} can be observed from the Gd_2O_2S:Tb powders ranging from 350 to 700 nm under X-ray excitation, which are due to transitions from the $^5D_{3,4}$ excited states to the ^7F_J (J=1–6) ground multiples[35-36,44]. The most prominent transition is in the spectral region of 545 nm ($^5D_4$-$^7F_5$ transition) giving rise to strong green emission. Fig. 5(b) shows the increase of luminous intensity in two stages, corresponding to the phase transition of the precursors respectively. The decrease of defect concentration of the Gd_2O_2S:Tb powders is one of the reasons for the increase of XEL intensity. The increasing proportion of S element in the precursors leads to the formation of more H_2S gas during the reduction, which effectively avoids Gd_2O_3 residue and inhibits the formation of S vacancies in the Gd_2O_2S:Tb powders. In addition, the improvement of

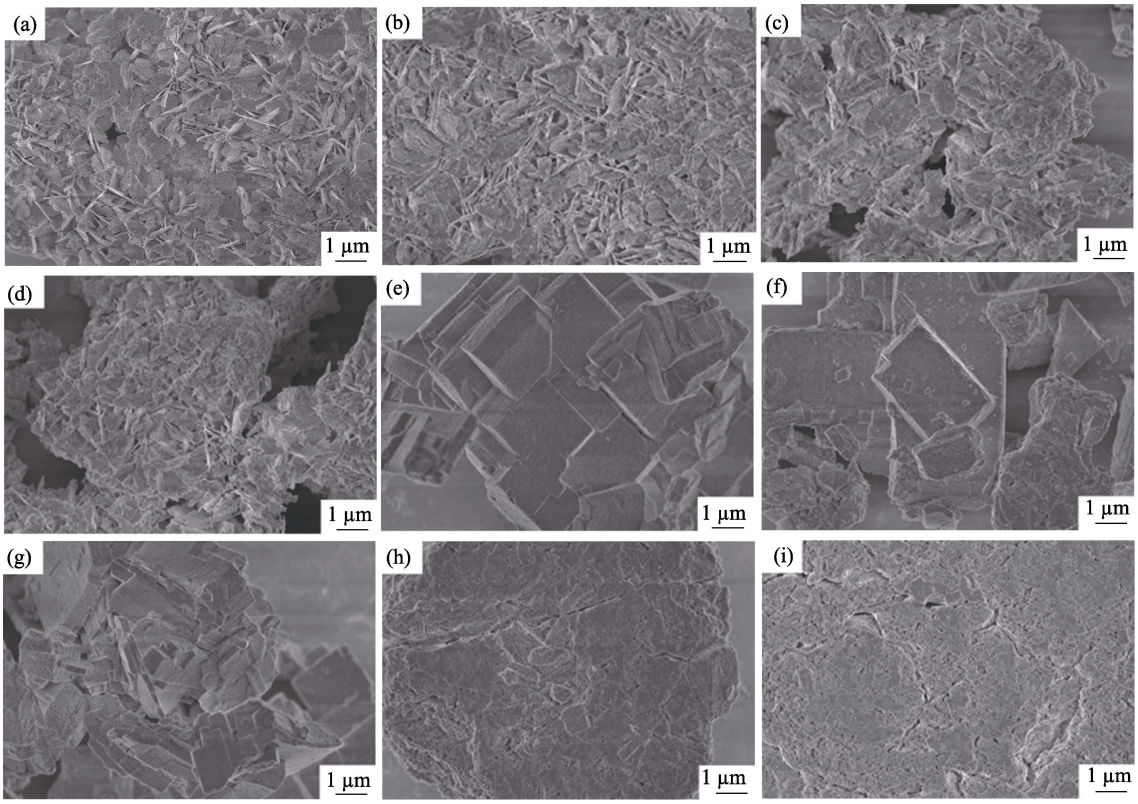

Fig. 4　FESEM morphologies of Gd_2O_2S: Tb powders with different n
(a) n=1.00; (b) n=1.25; (c) n=1.50; (d) n=1.75; (e) n=2.00; (f) n=2.25; (g) n=2.50; (h) n=2.75; (i) n=3.00

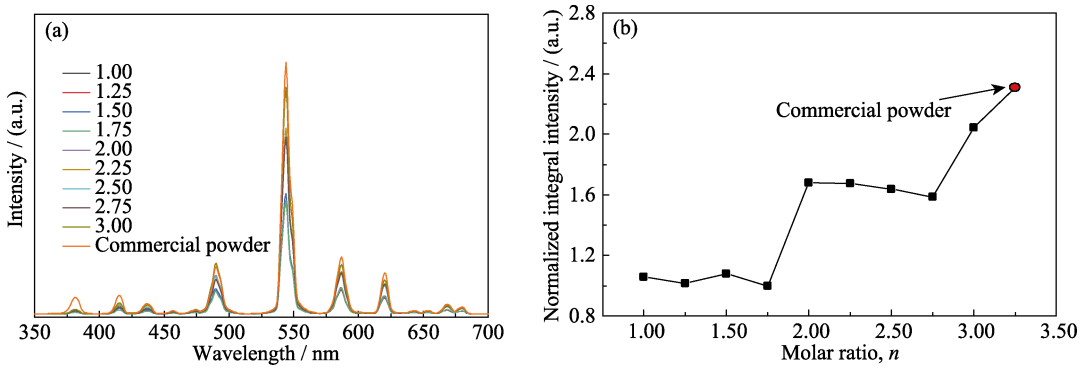

Fig. 5 XEL spectra and normalized integral intensity curves in the range of 350–700 nm of Gd_2O_2S:Tb powders with different *n*

(a) XEL spectra; (b) Normalized integral intensity curves; Colorful figures are available on website

particle crystallization and the growth of particle size of the powders also affect its luminescent properties, as shown in Fig. 3 and Fig. 4. It also can be seen from Fig. 5(b) that the XEL integral intensity in the range of 350–700 nm of Gd_2O_2S:Tb powders with n=3.00 is the closest to that of commercial micron powders, reaching 88% of XEL integral intensity of the commercial Gd_2O_2S:Tb powder. And the luminescent properties of the synthesized powder can be further improved by increasing the calcination temperature of the precursor to promote the crystallinity and grain growth.

Fig. 6 shows the relative densities of the Gd_2O_2S:Tb ceramics prepared with different *n* before and after HIP post-treatment. The relative densities of the pre-sintered ceramics decrease from 97.2% to 78.1% and then increase to 94.5% with *n* increasing from 1.00 to 3.00, corresponding to the morphology of the Gd_2O_2S:Tb powders changes, respectively. The result shows that the sintering activity of the powders is significantly affected by their morphologies. Compared to the Gd_2O_2S:Tb powder with block structure, the layered powders are easier to be broken in the molding process and the densification rate is faster. After the HIP post-treatment, the relative densities of all ceramics are increased. However, Gd_2O_2S:Tb ceramics prepared with n=2.00, 2.25 and 2.50 were still not densified. Therefore, the subsequent work can be considered to introduce the ball milling process to break the agglomeration of the powders in order to obtain high-density ceramics.

The EDS analysis was performed on Gd_2O_2S:Tb ceramics, as shown in Fig. 7. Two kinds of secondary phase can be found on the surface of the Gd_2O_2S:Tb ceramics. From the EDS analysis results, it can be seen that the secondary phase in the white area is Gd_2O_3. The secondary phase in the black area is aluminum-containing compound, which is introduced from the alumina crucible during the calcination and reduction of the powders. The black area on the ceramic surface increases significantly when n=3.00, indicating that the precursor of this component is more likely to introduce Al element, so the alumina crucible should be avoided when calcination and reduction of the powders.

The FESEM micrographs of the Gd_2O_2S:Tb ceramics vacuum pre-sintered at 1300 ℃ for 3 h and HIP post-treated at 1450 ℃ for 3 h are presented in Fig. 8. It can be seen that when n=2.00, 2.25 and 2.50, there are a lot of pores on the polished ceramics surface, indicating the ceramics are not completely compact. All ceramics have Gd_2O_3 secondary phase on the surface as mentioned above. When n<2.00, the surface of ceramics has relatively more secondary phase, and the distribution of the secondary phase does not decrease with the increase of *n*. This is because the composition of the precursor is consistent when n<2.00. The precursor is pure $Gd_2O_2SO_4$ after air calcination, and S element is not excessive during reduction. When 2.00≤n≤2.75, the distribution content of the secondary phase decreases, whichindicates the increase of S element proportion in the powders. The increase of *n* has a certain effect on the removal of the secondary phase in the ceramics, but theeffect is not significant. When n=3.00, the Gd_2O_3 secondary phase on the ceramic surface decreases obviously.

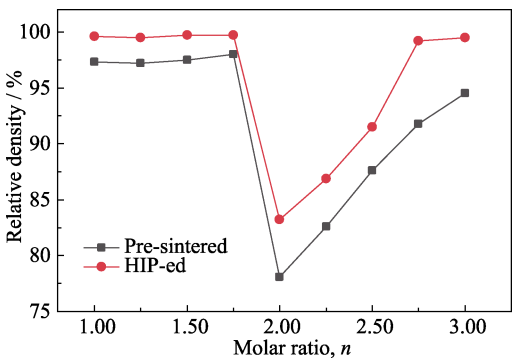

Fig. 6 Relative densities of Gd_2O_2S:Tb ceramics vacuum pre-sintered at 1300 ℃ for 3 h and HIP post-treatment at 1450 ℃ for 3 h fabricated from the powders with different *n*

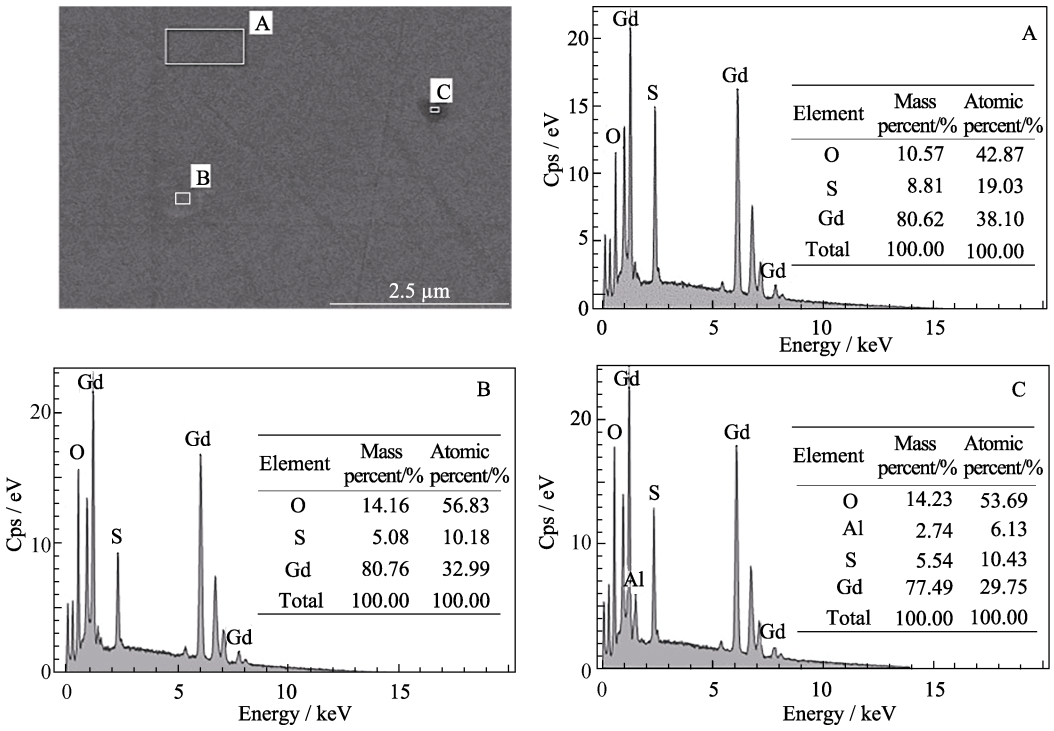

Fig. 7　FESEM micrograph and EDS patterns (white area) of the Gd_2O_2S:Tb ceramics vacuum pre-sintered at 1300 ℃ for 3 h and HIP post-treatment at 1450 ℃ for 3 h fabricated from the powders prepared with n=1.00

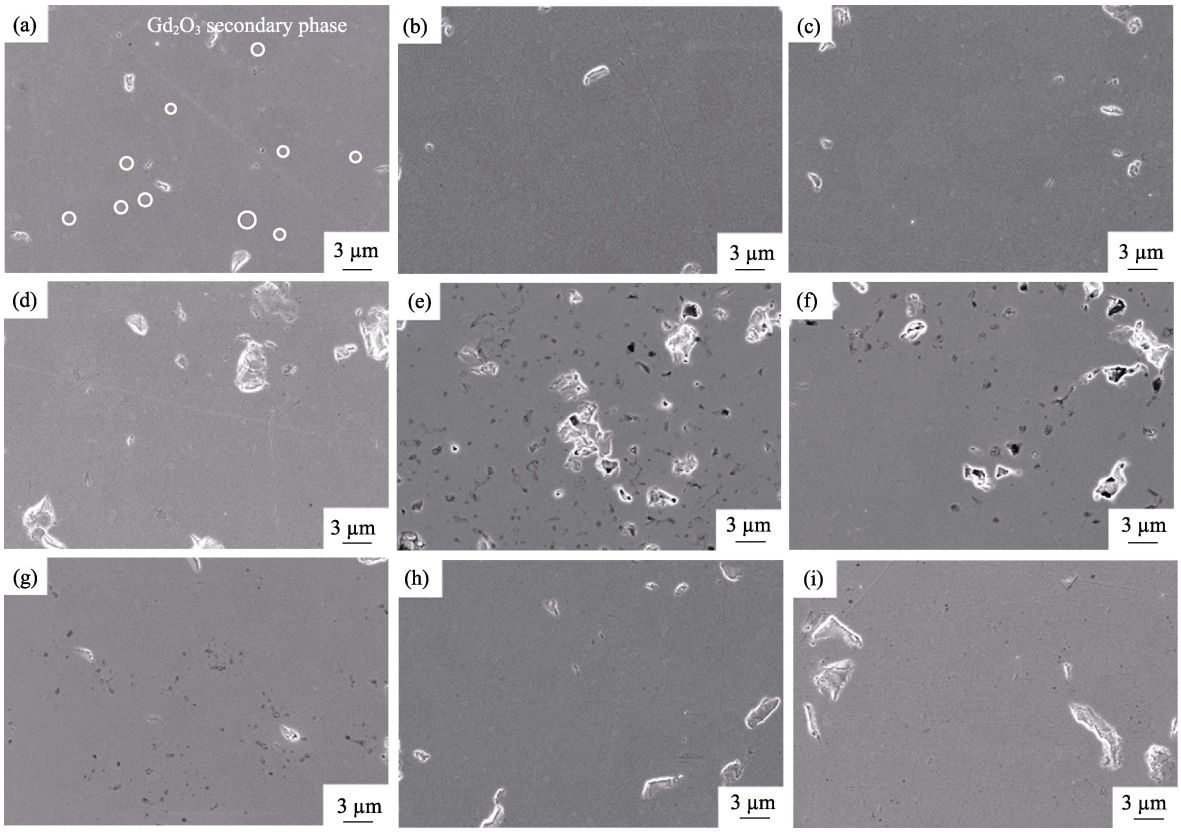

Fig. 8　FESEM morphologies of Gd_2O_2S:Tb ceramics fabricated from the powders prepared with different n
(a) n=1.00; (b) n=1.25; (c) n=1.50; (d) n=1.75; (e) n=2.00; (f) n=2.25; (g) n=2.50; (h) n=2.75; (i) n=3.00

The XEL spectra of Gd_2O_2S:Tb ceramics fabricated from the powders prepared with different n are shown in Fig. 9(a). The emission bands of the Gd_2O_2S:Tb ceramics in the range of 350–700 nm accords with the emission peaks of Tb^{3+}. The strongest emission peak centered at 545 nm corresponds to the $^5D_4$-$^7F_5$ transition[35,44]. The

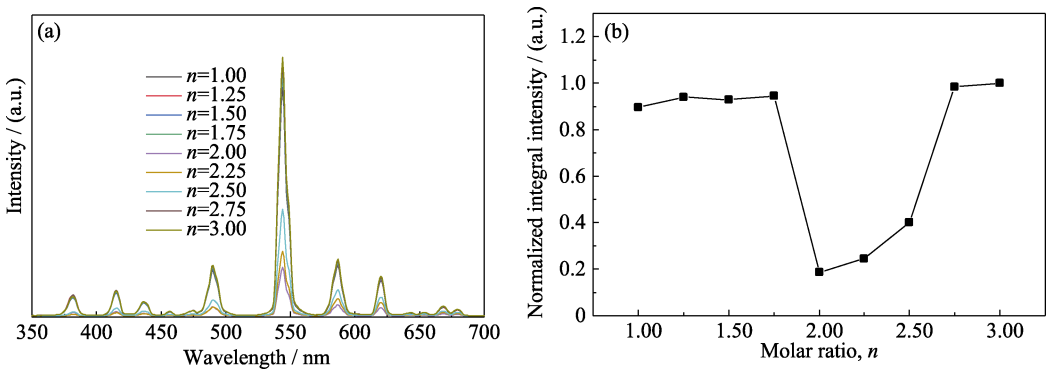

Fig. 9 XEL spectra and normalized integral intensity curves in the range of 350–700 nm of Gd_2O_2S:Tb ceramics fabricated from the powders with different *n*

(a) XEL spectra; (b) Normalized integral intensity curves; Colorful figures are available on website

normalized integral XEL intensity of Gd_2O_2S:Tb ceramics *versus* the powders *n* are shown in Fig. 9(b). For uncompact ceramics (*n*=2.00, 2.25, 2.50), the XEL intensity is relatively low, mainly due to the porosity. As the degree of densification of ceramics increases, the XEL intensity also gradually increases. For the compact ceramics (*n*=1.00, 1.25, 1.5, 1.75, 2.75 and 3.00), with the increase of *n*, the XEL intensity of the ceramic has a tendency to improve. But the secondary phase inside the ceramics will greatly reduce the scintillation performance of the ceramics. In addition, the ceramics has a higher XEL intensity when *n*=3.00, but there is no significant improvement compared with the ceramics fabricated from the powders prepared with other *n*. This is because more Al element may be introduced during the powders preparation, resulting in an increase in the content of aluminum-containing secondary phase in the ceramics.

3 Conclusions

The Gd_2O_2S:Tb precursors were synthesized with different molar ratios of H_2SO_4 to Gd_2O_3 in the hot water-bath. The Gd_2O_2S:Tb powders were obtained by reducing the precursors in H_2-Ar at 750 ℃. The chemical composition of the precursors and the products calcined in air changes with the increase of *n*. The chemical composition of the precursors can be described as $2Gd_2O_3{\cdot}Gd_2(SO_4)_3{\cdot}xH_2O$ ($n<2.00$), $Gd_2O_3{\cdot}2Gd_2(SO_4)_3{\cdot}xH_2O$ ($2.25 \leqslant n \leqslant 2.75$), $Gd_2(SO_4)_3{\cdot}8H_2O$ ($n=3$). After being calcined at 750 ℃ under a hydrogen atmosphere, all powders form pure phase Gd_2O_2S structure. The morphologies of the Gd_2O_2S:Tb powders are closely related to the phase composition of the precursor. With the increase of *n*, the XEL intensity of the Gd_2O_2S:Tb powders improves. The increase of the XEL intensity shows two stages, corresponding to the phase transition of the precursors respectively. Gd_2O_2S:Tb scintillation ceramics were fabricated by vacuum pre-sintering and HIP post-treatment in an Ar atmosphere. The ceramics fabricated from the powders prepared with different *n* achieve high relative density except the ceramics fabricated from the powders with block structure (*n*=2.00, 2.25, 2.50). Only the dense ceramics achieve relatively high XEL intensity. Two kinds of secondary phase which is Gd_2O_3 and aluminum-containing compound can be found on the surface of the Gd_2O_2S:Tb ceramics. The secondary phase seriously reduces the optical quality and scintillation property of the ceramics. The increase of *n* has a certain effect on the removal of the Gd_2O_3 secondary phase from the FESEM morphologies of Gd_2O_2S:Tb ceramics. Therefore, our subsequent work mainly focuses on the elimination of the secondary phase in the ceramics.

References:

[1] YANAGIDA T. Inorganic scintillating materials and scintillation detectors. *Proceedings of the Japan Academy Series B Physical and Biological Sciences*, 2018, **94(2):** 75.

[2] VAN EIJK C W E, BESSIèRE A, DORENBOS P. Inorganic thermal-neutron scintillators. *Nuclear Instruments and Methods in Physics Research Section A: Accelerators, Spectrometers, Detectors and Associated Equipment*, 2004, **529(1/2/3):** 260.

[3] LI J, XIE T F, KOU H M, *et al.* Effect of trace SiO_2 addition on optical and scintillation property of Pr:$Lu_3Al_5O_{12}$ ceramics. *Journal of Inorganic Materials*, 2019, **35(7):** 796.

[4] IKESUE A. Processing of Ceramics: Breakthroughs in Optical Materials. New York: Wiley, 2021**:** 73–141.

[5] QU Z X, YU C J, WEI Y T, *et al.* Thermal conductivity of boron carbide under fast neutron irradiation. *Journal of Advanced Ceramics*, 2022, **11(3):** 482.

[6] KHARIEKY A A, EBRAHIM SARAEE K R. Synthesis and characterization of radio and thermoluminescence properties of Sm doped Gd_2O_3, Gd_2O_2S and $Gd_2O_2SO_4$ nanocrystalline phosphors. *Journal of Luminescence*, 2020, **220:** 116979.

[7] QIAN B F, WANG Y L, ZHAO Q R, *et al.* Adjustable multi-color luminescence and energy transfer of capsule-shaped Gd_2O_2S: Tb^{3+}, Sm^{3+} phosphors. *Journal of Luminescence*, 2022, **244:** 118715.

[8] WANG W, KOU H M, LIU S P, *et al.* Optical and scintillation properties of Gd_2O_2S: Pr, Ce, F ceramics fabricated by spark plasma sintering. *Ceramics International*, 2015, **41(2):** 2576.

[9] BLAHUTA S, VIANA B, BESSIèRE A, *et al.* Luminescence quenching processes in $Gd_2O_2S:Pr^{3+},Ce^{3+}$ scintillating ceramics. *Optical Materials*, 2011, **33(10):** 1514.

[10] WANG W, KOU H M, LIU S P, *et al.* Comparison of the optical and scintillation properties of Gd_2O_2S: Pr, Ce ceramics fabricated by hot pressing and pressureless sintering. *Optical Materials*, 2015, **42:** 199.

[11] BAGHERI A, REZAEE EBRAHIM SARAEE K, SHAKUR H R, *et al.* Synthesis and characterization of physical properties of $Gd_2O_2S:Pr^{3+}$ semi-nanoflower phosphor. *Applied Physics A*, 2016, **122(5):** 553.

[12] POPOVICI E J, MURESAN L, HRISTEA-SIMOC A, *et al.* Synthesis and characterisation of rare earth oxysulphide phosphors. I. Studies on the preparation of Gd_2O_2S:Tb phosphor by the flux method. *Optical Materials*, 2004, **27(3):** 559.

[13] ZHAN Y H, AI F R, CHEN F, *et al.* Intrinsically zirconium-89 labeled Gd_2O_2S:Eu nanoprobes for *in vivo* positron emission tomography and gamma-ray-induced radioluminescence imaging. *Small*, 2016, **12(21):** 2872.

[14] TRTIK P, HOVIND J, GRüNZWEIG C, *et al.* Improving the spatial resolution of neutron imaging at Paul Scherrer Institut-The Neutron Microscope Project. *Physics Procedia*, 2015, **69:** 169.

[15] WANG F, YANG B, ZHANG J C, *et al.* Highly enhanced luminescence of Tb^{3+}-activated gadolinium oxysulfide phosphor by doping with Zn^{2+} ions. *Journal of Luminescence*, 2010, **130(3):** 473.

[16] CHEN L, WU Y, HUO H Y, *et al.* Nanoscale Gd_2O_2S:Tb scintillators for high-resolution fluorescent imaging of cold neutrons. *ACS Applied Nano Materials*, 2022, **5(6):** 8440.

[17] KANDARAKIS I, CAVOURAS D. Experimental and theoretical assessment of the performance of Gd_2O_2S:Tb and La_2O_2S:Tb phosphors and Gd_2O_2S:Tb-La_2O_2S:Tb mixtures for X-ray imaging. *European Radiology*, 2001, **11(6):** 1083.

[18] TRTIK P, LEHMANN E H. Progress in high-resolution neutron imaging at the Paul Scherrer Institut-The Neutron Microscope Project. *Journal of Physics: Conference Series*, 2016, **746:** 012004.

[19] YAN X, FERN G R, WITHNALL R, *et al.* Effects of the host lattice and doping concentration on the colour of Tb^{3+} cation emission in $Y_2O_2S:Tb^{3+}$ and $Gd_2O_2S:Tb^{3+}$ nanometer sized phosphor particles. *Nanoscale*, 2013, **5(18):** 8640.

[20] GIAKOUMAKIS G E, NOMICOS C D, SANDILOS P X. Absolute efficiency of Gd_2O_2S:Tb screens under fluoroscopic conditions. *Physics in Medicine and Biology*, 1989, **34(6):** 673.

[21] WESTPHAL E R, BROWN A D, QUINTANA E C, *et al.* Visible emission spectra of thermographic phosphors under X-ray excitation. *Measurement Science and Technology*, 2021, **32(9):** 094008.

[22] WANG W, LI Y S, KOU H M, *et al.* Gd_2O_2S: Pr scintillation ceramics from powder synthesized by a novel carbothermal reduction method. *Journal of the American Ceramic Society*, 2015, **98(7):** 2159.

[23] TRTIK P, LEHMANN E H. Isotopically-enriched gadolinium-157 oxysulfide scintillator screens for the high-resolution neutron imaging. *Nuclear Instruments and Methods in Physics Research Section A: Accelerators, Spectrometers, Detectors and Associated Equipment*, 2015, **788:** 67.

[24] YASUDA R, KATAGIRI M, MATSUBAYASHI M. Influence of powder particle size and scintillator layer thickness on the performance of Gd_2O_2S:Tb scintillators for neutron imaging. *Nuclear Instruments and Methods in Physics Research Section A: Accelerators, Spectrometers, Detectors and Associated Equipment*, 2012, **680:** 139.

[25] KATARIA V, MEHTA D S. Multispectral harvesting rare-earth oxysulphide based highly efficient transparent luminescent solar concentrator. *Journal of Rare Earths*, 2022, **40(1):** 41.

[26] HUANG X Y, DING J Y, LI J. Rare earth doped Gd_2O_2S scintillation ceramics. *Journal of Inorganic Materials*, 2021, **36(8):** 789.

[27] DANIEL J H, SAWANT A, TEEPE M, *et al.* Fabrication of high aspect-ratio polymer microstructures for large-area electronic portal X-ray imagers. *Sensors and Actuators A-Physical*, 2007, **140(2):** 185.

[28] WU G Q, QIN H M, FENG S W, *et al.* Ultrafine Gd_2O_2S:Pr powders prepared *via* urea precipitation method using SO_2/SO_4^{2-} as sulfuration agent—a comparative study. *Powder Technology*, 2017, **305:** 382.

[29] HE C, XIA Z G, LIU Q L. Microwave solid state synthesis and luminescence properties of green-emitting $Gd_2O_2S:Tb^{3+}$ phosphor. *Optical Materials*, 2015, **42:** 11.

[30] PEARSON R G. Hard and soft acids and bases. *Journal of the American Chemical Society*, 1963, **85(22):** 3533.

[31] DING Y J, HAN P D, WANG L X, *et al.* Preparation, morphology and luminescence properties of Gd_2O_2S:Tb with different Gd_2O_3 raw materials. *Rare Metals*, 2015, **38(3):** 221.

[32] SONG Y H, YOU H P, HUANG Y J, *et al.* Highly uniform and monodisperse $Gd_2O_2S:Ln^{3+}$ (Ln = Eu, Tb) submicrospheres: solvothermal synthesis and luminescence properties. *Inorganic Chemistry*, 2010, **49(24):** 11499.

[33] HAN P D, ZHANG L, WANG L X, *et al.* Investigation on the amounts of Na_2CO_3 and sulphur to obtain pure Y_2O_2S and up-conversion luminescence of Y_2O_2S:Er. *Journal of Rare Earths*, 2011, **29(9):** 849.

[34] LIU Q, PAN H M, CHEN X P, *et al.* Gd_2O_2S:Tb scintillation ceramics fabricated from high sinterability nanopowders *via* hydrogen reduction. *Optical Materials*, 2019, **94:** 299.

[35] WANG X J, MENG Q H, LI M T, *et al.* A low temperature approach for photo/cathodoluminescent Gd_2O_2S:Tb (GOS:Tb) nanophosphors. *Journal of the American Ceramic Society*, 2018, **102(6):** 3296.

[36] LIU Q, WU F, CHEN X P, *et al.* Fabrication of Gd_2O_2S:Pr scintillation ceramics from water-bath synthesized nanopowders. *Optical Materials*, 2020, **104:** 109946.

[37] WANG X J, WANG X J, WANG Z H, *et al.* Photo/catho-doluminescence and stability of Gd_2O_2S:Tb,Pr green phosphor hexagons calcined from layered hydroxide sulfate. *Journal of the American Ceramic Society*, 2018, **101(12):** 5477.

[38] PAN H M, LIU Q, CHEN X P, *et al.* Fabrication and properties of Gd_2O_2S:Tb scintillation ceramics for the high-resolution neutron imaging. *Optical Materials*, 2020, **105:** 109909.

[39] WANG X J, LI J G, MOLOKEEV M S, *et al.* Layered hydroxyl sulfate: controlled crystallization, structure analysis, and green derivation of multi-color luminescent $(La,RE)_2O_2SO_4$ and $(La,RE)_2O_2S$ phosphors (RE=Pr, Sm, Eu, Tb, and Dy). *Chemical Engineering Journal*, 2016, **302:** 577.

[40] WANG X, LI J G, ZHU Q, *et al.* Facile and green synthesis of $(La_{0.95}Eu_{0.05})_2O_2S$ red phosphors with sulfate-ion pillared layered hydroxides as a new type of precursor: controlled hydrothermal processing, phase evolution and photoluminescence. *Science and Technology of Advanced Materials*, 2014, **15(1):** 014204.

[41] JIANG P, LI Z P, LU W, *et al.* The pH value control of morphology and luminescence properties of Gd_2O_2S: Tb^{3+} phosphors. *Materials*, 2022, **15(2):** 646.

[42] LEPPERT J. Method for Producing Rare Earth Oxysulfide Powder. United States, C01F17/00, US6296824B1. 2001.10.02.

[43] TERAZAWA S, NITTA H. Production Method of Rare Earth Oxysulfide, Ceramic Scintillator and Its Production Method,

Scintillator Array, and Radiation Detector. United States, C09K 11/77, US9896623B2. 2018.02.20.
[44] PAWLIK N, SZPIKOWSKA-SROKA B, PIETRASIK E, *et al.* Photoluminescence and energy transfer in transparent glass-ceramics based on GdF_3:RE^{3+} (RE = Tb, Eu) nanocrystals. *Journal of Rare Earths*, 2019, **37(11):** 1137.

Gd_2O_2S:Tb 闪烁陶瓷的制备与结构: 水浴合成中 H_2SO_4/Gd_2O_3 摩尔比的影响

吴俊林[1,2], 丁继扬[1,3], 黄新友[3], 朱丹阳[1,2], 黄 东[1,3], 代正发[1], 杨文钦[4,5], 蒋兴奋[4,5], 周健荣[4,5], 孙志嘉[4,5], 李 江[1,2]

(1. 中国科学院 上海硅酸盐研究所, 透明光功能无机材料重点实验室, 上海 201899; 2. 中国科学院大学 材料科学与光电工程中心, 北京 100049; 3. 江苏大学 材料科学与工程学院, 镇江 212013; 4. 散裂中子源科学中心, 东莞 523803; 5. 中国科学院 高能物理研究所, 核探测与核电子学国家重点实验室, 北京 100049)

摘 要: Gd_2O_2S:Tb 闪烁陶瓷以其明亮的绿色发光、高能量转换效率和高中子俘获截面而广泛应用于中子成像和工业无损检测等领域, 但 Gd_2O_2S:Tb 陶瓷中存在的 Gd_2O_3 第二相影响其闪烁性能。本工作以 H_2SO_4 和 Gd_2O_3 为原料, 采用水浴法合成 Gd_2O_2S:Tb 前驱体, 研究了 H_2SO_4 与 Gd_2O_3 的摩尔比(n)对前驱体和 Gd_2O_2S:Tb 粉体性能的影响。前驱体的化学组成随 n 增大而变化: $2Gd_2O_3{\cdot}Gd_2(SO_4)_3{\cdot}xH_2O$($n$<2.00)、$Gd_2O_3{\cdot}2Gd_2(SO_4)_3{\cdot}xH_2O$ (2.25≤n≤2.75)和 $Gd_2(SO_4)_3{\cdot}8H_2O$(n=3.00), 经过空气煅烧和氢气还原后, 所有的粉体均形成 Gd_2O_2S 相。Gd_2O_2S:Tb 粉体的形貌与前驱体的相组成密切相关, 随着 n 增大, Gd_2O_2S:Tb 粉体的 XEL 强度增加呈现出两个阶段, 对应前驱体的相转变阶段。采用真空预烧结合热等静压烧结制备了 Gd_2O_2S:Tb 陶瓷, 相较于 n 为 2.00、2.25、2.50, 其他 n 制备的 Gd_2O_2S:Tb 陶瓷都达到了较高的相对密度和 XEL 强度, 不同 n 制备的陶瓷中都存在 Gd_2O_3 第二相, n 增大有利于减少陶瓷内部的第二相, 为进一步消除 Gd_2O_2S:Tb 陶瓷中的第二相提供了思路。

关 键 词: 水浴法; H_2SO_4 与 Gd_2O_3 摩尔比; Gd_2O_2S:Tb 纳米粉体; 闪烁陶瓷

中图分类号: TQ174 **文献标志码:** A